https://doi.org/10.1016/j.sab.2020.105794

Nanoparticle enhanced laser ablation and consequent effects on laser induced plasma optical emission

Alessandro De Giacomo*[1,2], Rim Alrifai[1], Vincent Gardette[1], Zita Salajkova[1,3], Marcella Dell'Aglio[2]

1. University of Bari, Department of Chemistry, Via Orabona 4, 70126 Bari-Italy

2. CNR-NANOTEC c/o Chemistry Department, University of Bari, Via Orabona 4, 70126 Bari, Italy

3. Central European Institute of Technology (CEITEC), Brno University of Technology, Purkyňova 656/123, 612 00 Brno, Czech Republic

**Corresponding author: Alessandro De Giacomo, email: alessandro.degiacomo@uniba.it*

Abstract

In this paper the plasmon enhanced ablation for elemental analysis is investigated with several experiments in order to point out the crucial questions concerning the laser matter interaction under the effect of plasmonic coupling between the nanoparticle (NP) system and the laser ablation pulse. The correlation between the electromagnetic field enhancement and the signal enhancement during NP enhanced laser induced breakdown spectroscopy (NELIBS), as well as the laser matter interaction at the nanoscale, is discussed in the case of noble metal NPs deposited on metal samples. The results suggest that, while laser pulse energy is concentrated in the space between the NPs, the NP system is shielded by the field enhancement distribution after the laser pulse interacts with the plasmons of the NP system. Finally the comparison of the laser energy transfer to the sample between NELIBS and conventional LIBS is discussed.

Keywords: Nanoparticle enhanced laser induced breakdown spectroscopy (NELIBS), plasmonic enhanced ablation, laser ablation, LIBS, LA-ICP-MS.

1. Introduction

Recently the use of nanoparticles (NPs) for improving laser ablation techniques in elemental analysis is getting a growing interest in analytical spectroscopy [1, 2]. Several applications have already been reported in literature and the number of papers on nanoparticle enhanced ablation for atomic spectrometry is still growing [1, 3-5]. In spite of the interest in taking advantage of the increased sensitivity with the use of NPs, few works are devoted to the understanding of the mechanisms by which the sensitivity enhancement is obtained. So far two main reasons have been discussed in literature about the emission enhancement during nanoparticle enhanced laser induced breakdown spectroscopy (NELIBS). One ascribes the emission enhancement to the lowering of the breakdown threshold obtained as a consequence of the different thermal properties between bulk samples and nanostructured materials [6]. This approach, although it may

be reasonable for sintered nanomaterial or for under-threshold ablation, cannot explain quantitatively the NELIBS enhancement obtained by many authors [1,7 and references therein]. A more reliable explanation of the NELIBS enhancement may be related to the plasmonic properties of NPs [1,8-9]. The effect of the coupling of the plasmonic system of NPs deposited on a flat surface with laser has been already discussed in several applications concerning surface enhanced raman scattering (SERS) or the electron emission with fs irradiation [10-11]. The case of NP enhanced photo ablation is different than the above mentioned examples, because the employed energy is in the regime of material breakdown and different questions need to be discussed. For example, how can the plasmonic system couple with the incident laser if the incoming energy is higher than the breakdown threshold of the metal constituting the nanostructures? Why is there no correlation between the ablated mass and the observed intensity enhancement? What is the relationship between the field enhancement and the observed NELIBS enhancement?

In this paper, although a lot of work still need to be done to fully understand the phenomena related to plasmon enhanced ablation, a set of dedicated experiments have been performed in order to try to answer the questions posed above in the easiest case of nanoparticle enhanced ablation of metallic targets. In this view, the following discussion is aimed to clarify and, at least, to indicate the crucial issues that need to be investigated for the understanding of the mechanisms allowing the plasmon enhanced ablation.

2. Experimental Set-up

The experiments were performed by using a Nd:YAG laser, Quantel Q-smart 850, with a pulse duration of 6 ns operating at 1064 nm with energies up to 850 mJ. In the case of the measurements of the breakdown threshold, the initial energy of the laser was reduced by reflecting a part of the beam with mirror in a range from 0.011 to 0.110 J. The spectrometer was a Czerny-Turner spectrograph (JY Triax 550) coupled with an ICCD (JY 3000) which was synchronized with the laser source by a pulse generator (Stanford DG 535) for doing emission spectroscopy of the plasma. The imaging system and a fast ICCD (New iStar, Andor) for the temporal and spatial resolved plasma imaging were used. To acquire simultaneously the plasma images at two different wavelengths on the ICCD, a set of optics consisting of two 50/50 beam splitters, two mirrors and two band pass filters were employed as described in detail in Ref. [12].

The target was placed perpendicularly to the laser beam using a 100 mm focal length lens placed on a micrometric stage in order to change the spot size on the sample in a range from 500 μm up to 2 mm. The employed NPs are AuNPs and Ag NPs produced by pulsed laser ablation in liquid (PLAL) with concentration of the mother solution equal to 0.2 g L^{-1} and diameter around 10 nm. For investigating the effect of plasmonic NPs on the laser ablation, the colloidal solution was dropped on the target and gently dried with airflow as described previously [1]. Briefly, 1-2 μl of the AuNP or AgNP solution was deposited on the target surfaces, after 5 cleaning laser shots. After drying, the deposited AuNP spot had a diameter of 2 mm and the laser was focused in the center of the spot. Specific experimental conditions are reported in the figure captions and in the text.

3. Results and discussion

3.1. Plasmon enhanced electromagnetic field and NELIBS enhancement.

According to the NP plasmon theory, the enhancement of the electromagnetic field is obtained in the portion of space between the NPs, acting as extremely efficient dipoles, when an incident electromagnetic field, is in resonance with the surface plasmonic band [13, 14]. This electromagnetic field enhancement is

localized among the induced coherent dipoles in a small volume between the NPs (i.e., a “hot spot”). The magnitude of the enhancement depends on the inverse of the cube of the interparticle distance [15, 16].

A previous paper [17] shows, that, when noble metal NPs are deposited on a metallic substrate, the resonance band of the plasmonic system broadens by several hundred nanometers and its peak is located in near infrared (Fig.1). This allows a good matching between the electromagnetic field of the Nd:YAG laser pulse at 1064 nm and the one induced on the NP system. Moreover the same paper reports that the coupling of the plasmons of the NP system with the surface plasmon of the metal substrate introduces additional hot spots close to the sample surface. The latter result is related to the different NELIBS efficiency observed between metallic samples and dielectric ones [1, 18]. As already reported [1], the enhancement of the emission signal due to plasmon enhanced ablation-based techniques strongly depends on the surface concentration of NPs because it is directly correlated to the average distance between the NPs deposited on the sample surface. In Fig.2 the experimental enhancement during a NELIBS experiment on metallic titanium with gold NPs is reported as function of the average distance between NPs, as calculated from the experimental surface concentration. The emission enhancement (EN) is due to the following equation [18]:

$$EN = \frac{I_{NELIBS}}{I_{LIBS}} = \frac{N_{0,\ NELIBS}}{N_{0,\ LIBS}} \frac{Z(T_{LIBS})}{Z(T_{NELIBS})} exp\left[\frac{E_u}{k}\left(\frac{1}{T_{LIBS}} - \frac{1}{T_{NELIBS}}\right)\right] \approx \frac{N_{0,\ NELIBS}}{N_{0,\ LIBS}} \qquad \text{Eq.1}$$

Where I is the intensity, Z(T) the partition function, T the temperature, E_u the energy of the upper level and N_0 the total number density of emitters, as indicated in the subscript, respectively for LIBS and NELIBS.

If we neglect the small difference in temperature [18] between LIBS and NELIBS, the NELIBS enhancement is mainly given by the different amount of emitters in the plasma when plasmon enhanced ablation is enabled. Here we should anticipate that the higher number of emitters does not necessarily imply a higher ablation mass. Indeed the number of emitters reported in Eq. 1 refers to the number of atoms that take part in the excited state distribution function of the species. The latter depends on the extent of atomization and excitation of the ejected mass.

On the other hand, we can calculate the enhancement of the electromagnetic field (EN_{em}), after the coupling of the laser pulse with the plasmonic system, with respect to the incident laser pulse electromagnetic field with the following equation:

$$EN_{em} = \frac{E_p}{E_0} = 1 + \frac{\mu'}{2\pi\varepsilon_d\varepsilon_0 D^3 E_0} \qquad \text{Eq. 2}$$

Where E_0 is the incident electromagnetic field, E_P is the is the electromagnetic field induced on the NPs system, $\varepsilon_d\varepsilon_0$ the permittivity of the air, D is the interparticle distance and μ’ is the dipole of the NP system calculated with the following equation [16, 19]:

$$\mu' = \varepsilon_0\varepsilon_d\alpha' E_0 \qquad \text{Eq. 3}$$

α’ is the polarizability given by:

$$\alpha' = \frac{2\pi r_{NP}^2(\varepsilon_m - \varepsilon_d)}{\varepsilon_m\left(4 - \frac{(2r_{NP})^3}{D^3}\right) + \varepsilon_d\left(8 - \frac{(2r_{NP})^3}{D^3}\right)} \quad \text{Eq. 4}$$

Where ε_m is the metal permittivity and r_{NP} is the radius of the NP.

Fig.2 shows the electromagnetic field enhancement according to the Eq.2 as function of the averaged interparticle distance, assuming ε_m is -1.9. By the inspection of Fig.2, it can be noted that there is a direct proportionality between the NELIBS enhancement and the electromagnetic field enhancement as both of these physical quantities depend on D^{-3}. Clearly in Eq.2, being purely theoretical, the field enhancement asymptotically tends to infinity for null distance (dashed line). As a matter of fact strong losses occur when the electromagnetic field in between the NPs is too high, and this is observed experimentally (solid circles) as a leveling off of the curve. As an example in Fig.2 we included a correction to the electromagnetic field for the tunnel effect (open squares). The correction is based on the dependence of the probability of the tunnel effect as function of the electromagnetic field (see Eq. S1-3 in the supporting information) and assumes that when the tunneling between the NPs occurs the plasmonic system is partially compromised as a consequence of the unbalancing of the plasmon oscillation forces. In Fig.2 it can be noted that, adding this correction, a levelling off of the electromagnetic field enhancement is obtained, similar to the experimental results. This explains the fact that below a certain interparticle distance, although the electromagnetic field should still increase, the NELIBS enhancement does not.

In any case, when considering the relationship between the NELIBS enhancement and the plasmon enhanced electromagnetic field, we should take into consideration that the laser pulse energy is the only energy furnished to the sample system. This means that, although under the effect of the NP plasmon resonance the energy is enhanced in the hot spots, the total energy delivered to the sample is the same during NELIBS and LIBS. That means, that in the case of metals, where hot spots are located close to the sample, an extremely efficient transfer of energy from the laser to the sample is obtained in the surrounding zone of the NPs. As the laser energy is converted into electronic excitation inside the sample, the effect of the energy concentration in between the NPs is localized in the hot spot on the sample surface only at the very beginning of the laser pulse irradiation. Then it immediately spreads throughout the irradiated portion of sample. This simple observation implies two important considerations:

1) If the energy of the laser is concentrated in some specific part of the irradiated sample (i.e., in the space between the NPs), the energy deposited on the NPs themselves must be strongly reduced in order to hold the total energy deposited on the sample constant and equal to the energy of the laser pulse.
2) As the ablation mass mainly depends on the effective energy deposited on the sample, if the same laser pulse characteristics are employed during a NELIBS and a LIBS experiment and the difference of the average optical properties along the laser spot area with and without NPs deposition is negligible, no important differences should be expected in the ablation mass as reported in Ref.[20].

3.2 Distribution of laser energy during plasmon enhanced laser ablation

The laser energy at certain fluence, F, with laser spot of radius R is given by:

$$E_{laser} = F \cdot \pi R^2 \quad \text{Eq. 5}$$

According to the consideration of the previous section this energy will be distributed in the hot spots and on the NPs surrounding the hot spots. The energy concentrated in the hot spot can be estimated with the following equation:

$$E_{hot} = \alpha E N^2 F \pi r_{hot}^2 N_{NP} \quad \text{Eq. 6}$$

In the following equation α is a proportionality factor that takes into account the NP coupling efficiency, r_{hot} is the radius of the hot spot and N_{NP} is the number of irradiated NPs. In Eq. 6 it is used EN^2, as the enhancement is proportional to the electromagnetic field induced on the NP system (see Fig.2) rather than its energy. As will be discussed later, this observation suggests that the effect of the NPs deposited on the sample does not affect the energy of the emitted radiation from the plasma, but it affects the number of emitters as a consequence of a more efficient atomization and excitation of the ablated sample during the laser-matter interaction stage.

The residual energy that is not focused in the hot spot and that interacts directly with the NPs can be estimated as the difference between the total laser energy and the E_{hot}

$$E_{residual} = E_{laser} - E_{hot} = \pi F\left(R^2 - \alpha E N^2 r_{hot}^2 N_{NP}\right) \quad \text{Eq.7}$$

so the residual energy on a single NP of radius r_{NP} is given by:

$$E_{NP} = E_{residual}\frac{r_{NP}^2}{R^2} \quad \text{Eq.8}$$

If the residual energy is higher than the breakdown threshold of the metallic NP, then the NP is vaporized and the plasmonic enhanced ablation effect decreases. The breakdown threshold of the NP system is different than the one corresponding to the bulk metal. Although the boiling and vaporization temperatures of a single NP are lower than the corresponding bulk ones, the breakdown threshold is higher for the NP system with respect to the bulk one. To prove this, we have measured the breakdown threshold at 1064 nm of a bulk gold sample and of a gold NP system deposited on Teflon. The breakdown threshold was estimated by the method proposed in Ref. [21], reporting the signal to noise ratio of the emission line at 312.27 nm as function of the laser fluence (see supporting information). The resulting breakdown thresholds were 0.8 and 2.3 J cm^{-2} for Au bulk and 10 nm Au NPs, respectively that corresponds to an energy for each single NP of about 7 10^{-12}J. According to Eq.7, if an efficient plasmon coupling between the NPs occurs, the laser energy is mainly concentrated in the hot spots and, in turn, the density of energy on the NP surface is lower than that of the incident laser pulse. In other words the plasmonic effect is at the same time concentrating the laser energy in between the NPs and shielding the NPs themselves. As mentioned above, this is a crucial issue for having the ns plasmonic enhanced ablation, because the efficiency of the plasmons depends on the presence of the NPs during the pulse irradiation.

Fig. 3 reports, as an example, the residual energy per NP (dashed line) at the same experimental conditions of the experimental enhancement reported in Ref. [7] as listed in the caption, assuming r_{hot}=1nm. By the inspection of Fig. 3 it is possible to note, that at these experimental conditions, for fluence beyond 20 J cm^{-2}, the residual energy reaches the breakdown threshold of the NP and, according to the present discussion, the experimental NELIBS enhancement starts to decrease because the plasmonic system is losing dipoles components and consequently the efficiency of the plasmon enhanced ablation decreases.

According to Eq.7, the higher the enhancement the lower the residual energy on the NPs and this strongly depends on the quality of the NPs deposition on the sample surface, which, indeed, is the crucial issue in determining the efficiency of plasmon enhanced laser ablation [1, 7]. This also implies that the higher the enhancement that can be reached with NELIBS, the higher the laser fluence that can be employed.

3.3 Comparison of the mass ablated during conventional laser ablation and NP enhanced laser ablation

Previous work shows that, although the morphology of the laser induced craters during NP enhanced ablation and conventional ablation are very different [9,18,20, 22], the volume of the craters does not differ significantly [20]. To confirm this effect Fig.4a and b show the crater profiles during NELIBS and LIBS, and their corresponding spectra. The measurements were done with 50 laser shots with the delay of 1 minute between each other. In the case of NELIBS, after every shot the crater was cleaned and a new NP deposition was done. Then the reproducibility of the NELIBS signal was controlled with the emission spectrum and is around 75%. The obtained craters for a laser spot 2 mm in diameter were then observed with a profilometer. By the inspection of Fig.4a, although it is not possible to quantitatively compare the ablated volume from the profilometer measurements, the profile does not show any substantial difference, although the LIBS crater seems slightly bigger than the NELIBS one [20]. Despite similar crater depth, the emission signal of the NELIBS experiment is notably more intense than the LIBS one as reported in Fig.4b. It is interesting to note that with an enhancement of the net emission intensity (i.e., peak area with background subtraction) of NELIBS with respect to LIBS, the background continuum radiation is also increased in the NELIBS spectrum. This is because the continuum radiation at a delay time of 1 μs is due to radiative recombination, the intensity of which is proportional to the number of atoms produced by direct electron ion recombination that in the case of NELIBS is higher than in LIBS [7]. These results show that the NELIBS enhancement is not due to any difference in the ablation mass.

3.4 NPs in the plasma phase

The scanning electron microscope (SEM) image in Fig. 5 shows the surface of the Al based alloy target covered with AuNPs and includes (A) the crater after the laser ablation and (B) an adjacent zone where no interaction with the laser occurred. It is possible to note that after the laser pulse some of the NPs are still on the sample, holding the same size and shape, which suggests that they did not experience any transformation upon laser irradiation. Of course, the number is notably reduced as some of them have been covered by the melted and re-solidified sample, some of them have been pushed away by the shockwave and most of them have been processed in the plasma phase. To investigate this latter aspect the temporal emission of the NP atomic signal was investigated and compared with the emission of the atoms coming from the sample substrate. As an example, in Fig. 6 the emission lines of Ag I at 328.07 nm and of Ti I at 327.7 nm are reported as function of time during NELIBS of a titanium with AgNPs. It is clear that, while the emission signal of Ti I has the typical decreasing trend after the laser pulse, the silver

emission appears later and it reaches a maximum after 285 ns. This probably corresponds to the time of evaporation of the NPs is the plasma phase [23]. In Fig.7 the spectrally resolved emission images show again a different trend between the emission of Ag at 328.07 nm and of Al at 396.15 nm during NELIBS on an aluminum based alloy with silver NPs. In this case, it is interesting to note that the emission of silver in the time interval of 200-400 ns after the laser pulse is shifted forward in distance with respect to the emission of the Al I, denoting that initially the particles are on the front-head of the plasma. Assuming the same velocity for all the species in the plasma, the spatial shift of the silver implies a temporal delay in the silver emission with respect to aluminum, confirming the observation reported above.

The presence of the NPs during the laser-matter interaction for the whole laser pulse duration and the subsequent evaporation in the plasma phase suggests important issues concerning the NELIBS enhancement mechanisms. Assuming an initial expansion rate of the ablated matter between of 10^6- 10^7 cm s^{-1} (in agreement with ref. [24]) and an expansion shape that initially resembles an oblate spheroid (as shown in Fig.8) during the 6 ns laser pulse, the distance between NPs is still small enough to allow plasmon coupling between the NPs. Table 1 reports the calculated values of the interparticle distances at different initial expansion rates, considering an initial two-dimensional circular surface of 1 mm diameter (the laser spot), containing 10^{10} NPs of 20 nm diameter, that turns into an oblate spheroid surface with a major semi-axis equal to the spot radius and a minor semi-axis (a) equal to the distances covered by the ablated matter after the 6 ns laser pulse. Because efficient plasmon interaction occurs at interparticle distances on the same order or less than the particle diameter, by the inspection of Table 1 it is clear that at conventional expansion rates the plasmonic effect holds for the entire laser pulse duration. Now, assuming that the difference in the ablated mass between NELIBS and LIBS is negligible, this phenomenon can play a crucial role in the NELIBS effect and may be the way further energy is delivered to the ejected mass, improving the atomization and the excitation of the sample.

3.5 The emission intensity and the ablated mass

As it is well known, during laser ablation increasing the laser fluence, keeping constant the laser spot size, the ablated mass increases until a critical ejection of matter is reached [25]. After this stage, further energy does not reach the sample because the ablated matter, and especially the electrons, completely shield the target surface. This excess of energy is spent in exciting the ablated mass, inducing further atomization, ionization and excitation. In order to increase the flux of ejected matter for obtaining a higher quantity of ablated mass, it is necessary to hold the same fluence but enlarge the laser spot. In the latter case, although a larger portion of laser pulse energy reaches the target surface, as a consequence of the larger amount of ejected matter, the pulse energy per ablated mass can be not so efficient in exciting the ejected material as in the case of smaller spot size. This issue is shown in Fig. 9a and b, where the ablation mass measured by the crater profile (see supporting information) and the emission intensity of Ti I at 462.3nm are reported as function of laser energy, respectively. In Fig. 9a-b the data are reported keeping constant the spot size and varying the laser fluence (circles) and keeping constant the laser fluence but varying the spot size (squares). We can observe that keeping constant the laser spot to 500 µm, after some tens of mJ, the increase of the laser fluence does not have any noticeable effect, within experimental error, on the ablated mass However, in Fig.9b it can be observed that the intensity increases as a consequence of a better excitation of the ablated matter. Fig.9a also shows the effect on the ablation mass that is obtained increasing the laser spot size and keeping constant the laser fluence that leads also to a higher intensity in Fig. 9b, as a larger number of emitters is produced. To better clarify this point we introduce the relative emission efficiency, which is the ratio between the relative intensity and the ablated mass. The effect of the larger amount of ablated mass, as well as the effect of the energy spent for excitation, can be monitored

simultaneously, as reported in Fig.9c. By the inspection of Fig 9c we can see that, keeping constant the laser fluence and increasing the spot size, the LIBS emission efficiency decreases in spite of the higher ablated mass. On the contrary, the emission efficiency of NELIBS increases for increasing the spot size and, in turn, the ablated mass. These results suggest that NELIBS, although it does not increase the ablation mass, it allows a better atomization and excitation of the ejected material. In this view the plasmonic effect during the entire duration of the laser irradiation allows to deposit the energy on that part of the material that in conventional LIBS would not take part in the emission of radiation as it cannot interact efficiently with the laser pulse. As shown in Fig.9d the NELIBS enhancement increases with the amount of ablated material, but is negligible for low amounts of ejected material because in this case conventional LIBS is efficient enough to excite all of the ablated matter and no further energy is required to support the laser pulse.

Conclusion

In this paper some basic aspects of the nanoparticle enhanced ablation have been investigated in order to extend the knowledge on the fundamental mechanisms leading to the signal enhancement. The plasmonic nature of the signal enhancement during NELIBS has been proven experimentally by the correlation between the NELIBS enhancement and the electromagnetic field enhancement, as well as by the negligible difference in the ablated mass (as measured with profilometry) with respect to differences in emission intensity with and without plasmon enhanced ablation. On the basis of the conservation of energy and on the spectral features of the NP atomic emission lines during plasma evolution, the shielding of the NPs due to the plasmonic effect has been discussed. Finally the comparison of the laser pulse partition in NELIBS and LIBS has been discussed in terms of ablation mass and emission efficiency. The results reported in the present paper, although do not elucidate completely all the processes occurring during plasmon enhanced ablation, give a new insight on the reasons leading to NELIBS enhancement.

Acknowledgments: The authors are grateful to Dr. Vincent Motto Ros from the University of Lyon for the support in the spectral resolved images and to the group of Prof. Jozef Kaiser from CEITEC for taking part in the discussion and to Mr. Savino Cosmai and Dr. F. Palumbo from CNR-Nanotec for crater measurements and to Dr. J.B. Sirven and J.L. Lacour from CEA for the preliminary investigation on crater profiles and Prof. Annarosa Mangone from the University of Bari and Dr. Sarah Jantzi from the University of Georgia for taking part in the discussion.

Appendix A. Supplementary data' and 'Supplementary data to this article can be found online at doi:...

References

[1] M. Dell'Aglio, R. Alrifai, A. De Giacomo , Nanoparticle Enhanced Laser Induced Breakdown Spectroscopy (NELIBS), a first review. Spectrochimica Acta B, 2018, 148 105–112

[2] M. Holá, Z. Salajková, A. Hrdlička, P. Pořízka, K. Novotný, L. Čelko, P. Šperka, D. J. Novotný, P. Modlitbová, V. Kanický, J. Kaiser, Feasibility of Nanoparticle-Enhanced Laser Ablation Inductively Coupled Plasma Mass Spectrometry, Anal. Chem. 90 (20) (2018) 11820-11826

[3] Marcella Dell'Aglio, Zita Salajkova, Antonia Mallardi, Raffaele Mezzenga, Leonie van't Hag, Nicola Cioffi, Gerardo Palazzo, Alessandro De Giacomo, Application of gold nanoparticles embedded in the amyloids fibrils as enhancers in the laser induced breakdown spectroscopy for the metal quantification in microdroplets, Spectrochimica Acta Part B: Atomic Spectroscopy, Volume 155, 2019, 115-122.

[4] R.H. El-Saeid, Z. Abdel-Salam, S. Pagnotta, V. Palleschi, M.A. Harith, Classification of sedimentary and igneous rocks by laser induced breakdown spectroscopy and nanoparticle-enhanced laser induced breakdown spectroscopy combined with principal component analysis and graph theory, Spectrochimica Acta Part B: Atomic Spectroscopy, Volume 158, 2019, 105622.

[5] Zhao, X., Zhao, C., Du, X., Dong, D. Detecting and Mapping Harmful Chemicals in Fruit and Vegetables Using Nanoparticle-Enhanced Laser-Induced Breakdown Spectroscopy (2019) Scientific Reports, 9 (1), art. no. 906

[6] Ashraf M. EL Sherbini, Christian G. Parigger, Nano-material size dependent laser-plasma thresholds, Spectrochimica Acta Part B: Atomic Spectroscopy, Volume 124, 2016, 79-81.

[7] A. De Giacomo, M. Dell'Aglio, R. Gaudiuso, C. Koral, G. Valenza, Perspective on the use of nanoparticles to improve LIBS analytical performance: nanoparticle enhanced laser induced breakdown spectroscopy (NELIBS), J. Anal. At. Spectrom., 31 (2016) 1566-1573.

[8] Jie Shen, Keyan Wu, Da Cao, Jijin Wang, Bitao Hu, Effect of Ag nanoclusters deposited with magnetron sputtering on laser-induced breakdown spectroscopy enhancement, Spectrochimica Acta Part B: Atomic Spectroscopy, Volume 156, 2019, 59-65.

[9] Keyan Wu, Jie Shen, Da Cao, Huibo Cheng, Shaohua Sun, and Bitao Hu, Coulombic Effect of Amphiphiles with Metal Nanoparticles on Laser-Induced Breakdown Spectroscopy Enhancement, J. Phys. Chem. C 2018, 122, 19133−19138.

[10] Sharma, B., Frontiera, R.R., Henry, A.-I., Ringe, E., Van Duyne, R.P. SERS: Materials, applications, and the future (2012) Materials Today, 15 (1-2), pp. 16-25.

[11] F. Schertz, M. Schmelzeisen, M. Kreiter, H.J. Elmers, G. Schonhense, Field Emission Effect Generated by the Near Field of Strongly Coupled Plasmons, Physical review Letters (2012) 108, 237602, 1-5.

[12] Dell'aglio, M., Motto-Ros, V., Pelascini, F., Gornushkin, I.B., De Giacomo, A., Investigation on the material in the plasma phase by high temporally and spectrally resolved emission imaging during pulsed laser ablation in liquid (PLAL) for NPs production and consequent considerations on NPs formation

(2019) Plasma Sources Science and Technology, 28 (8), art. no. 085017

[13] Schuller, J.A., Barnard, E.S., Cai, W., Jun, Y.C., White, J.S., Brongersma, M.L. Plasmonics for extreme light concentration and manipulation (2010) Nature Materials, 9 (3), pp. 193-204.

[14] Halas, N.J., Lal, S., Chang, W.-S., Link, S., Nordlander, P. Plasmons in strongly coupled metallic nanostructures (2011) Chemical Reviews, 111 (6), pp. 3913-3961.

[15] Huang, Y., Ma, L., Hou, M., Li, J., Xie, Z., Zhang, Z. Hybridized plasmon modes and near-field enhancement of metallic nanoparticle-dimer on a mirror (2016) Scientific Reports, 6, art. no. 30011

[16] Amendola, V., Pilot, R., Frasconi, M., Maragò, O.M., Iatì, M.A. Surface plasmon resonance in gold nanoparticles: A review (2017) Journal of Physics Condensed Matter, 29 (20), art. no. 203002.

[17] De Giacomo, A., Salajkova, Z., Dell'aglio, M., A quantum chemistry approach based on the analogy with π-system in polymers for a rapid estimation of the resonance wavelength of nanoparticle systems (2019) Nanomaterials, 9 (7), art. no. 929.

[18] A. De Giacomo, R. Gaudiuso, C. Koral, M. Dell'Aglio, O. De Pascale, Nanoparticle Enhanced Laser Induced Breakdown Spectroscopy: Effect of nanoparticles deposited on sample surface on laser ablation and plasma emission, Spectrochimica Acta Part B: Atomic Spectroscopy, Volume 98, 2014, 19-27.

[19] Jain, P.K., El-Sayed, M.A. Noble metal nanoparticle Pairs: Effect of medium for enhanced nanosensing (2008) Nano Letters, 8 (12), pp. 4347-4352.

[20] Mangone, A., Mastrorocco, F., Giannossa, L.C., Comparelli, R., Dell'Aglio, M., De Giacomo, A., Nanoparticle enhanced laser ablation inductively coupled plasma mass spectrometry (2020) Spectrochimica Acta - Part B Atomic Spectroscopy, 163, art. no. 105731

[21] L.M. Cabalin, J.J. Laserna, Experimental determination of laser induced breakdown thresholds of metals under nanosecond Q-switched laser operation, Spectrochimica Acta Part B 53 (1998) 723-730.

[22] Mengmeng Wang, Lan Jiang, Sumei Wang, Qitong Guo, Feng Tian, Zhuyuan Chu, Jin Zhang, Xin Li, and Yongfeng Lu, Multiscale Visualization of Colloidal Particle Lens Array Mediated Plasma Dynamics for Dielectric Nanoparticle Enhanced Femtosecond Laser-Induced Breakdown Spectroscopy, Anal. Chem. 2019, 91, 9952−9961.

[23] Itina T E et al 2010 Laser applications for nanotechnology: insights from numerical modeling AIP Conf. Proc. 1278, 38–50.

[24] De Giacomo, A., Experimental characterization of metallic titanium-laser induced plasma by time and space resolved optical emission spectroscopy

(2003) Spectrochimica Acta - Part B Atomic Spectroscopy, 58 (1), pp. 71-83

[25] Ahmed M. Elsied, Payson C. Dieffenbach, Prasoon K. Diwakar, Ahmed Hassanein, Nanosecond laser-metal ablation at different ambient conditions, Spectrochimica Acta Part B: Atomic Spectroscopy, Volume 143, 2018, Pages 26-31

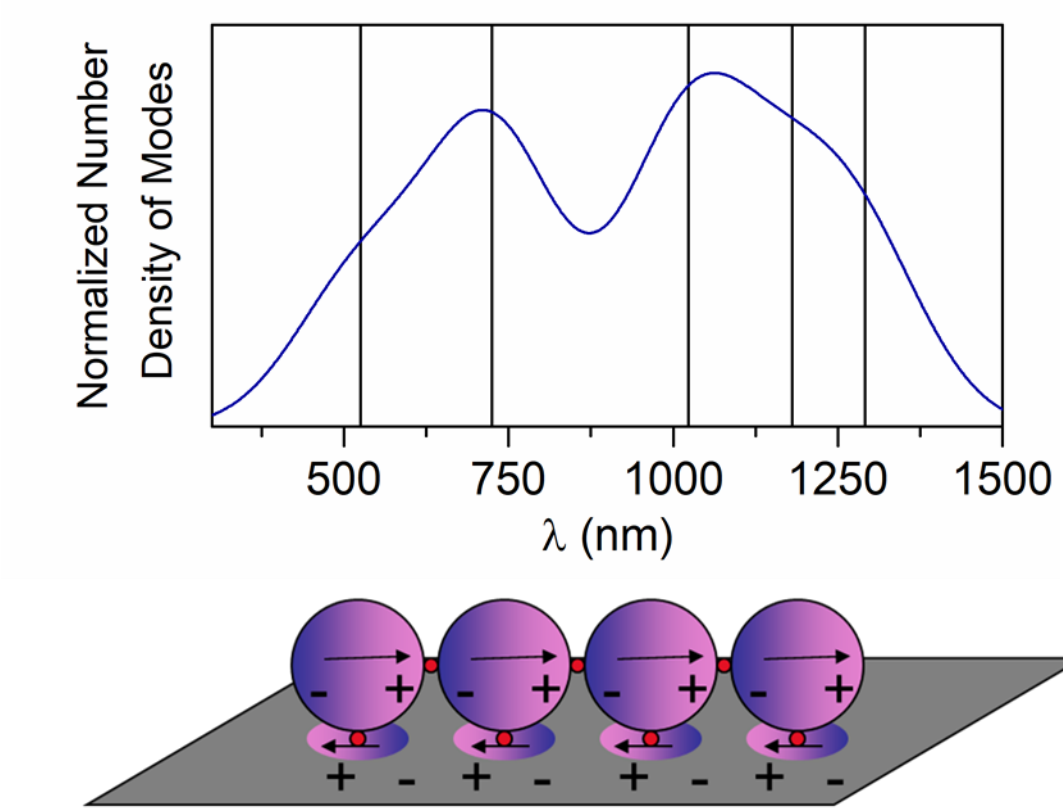

Fig.1 Diagram of plasmonic interactions between NPs and the metallic target surface. The red points indicate the generated hot spots and the purple balls are plasmons [17].

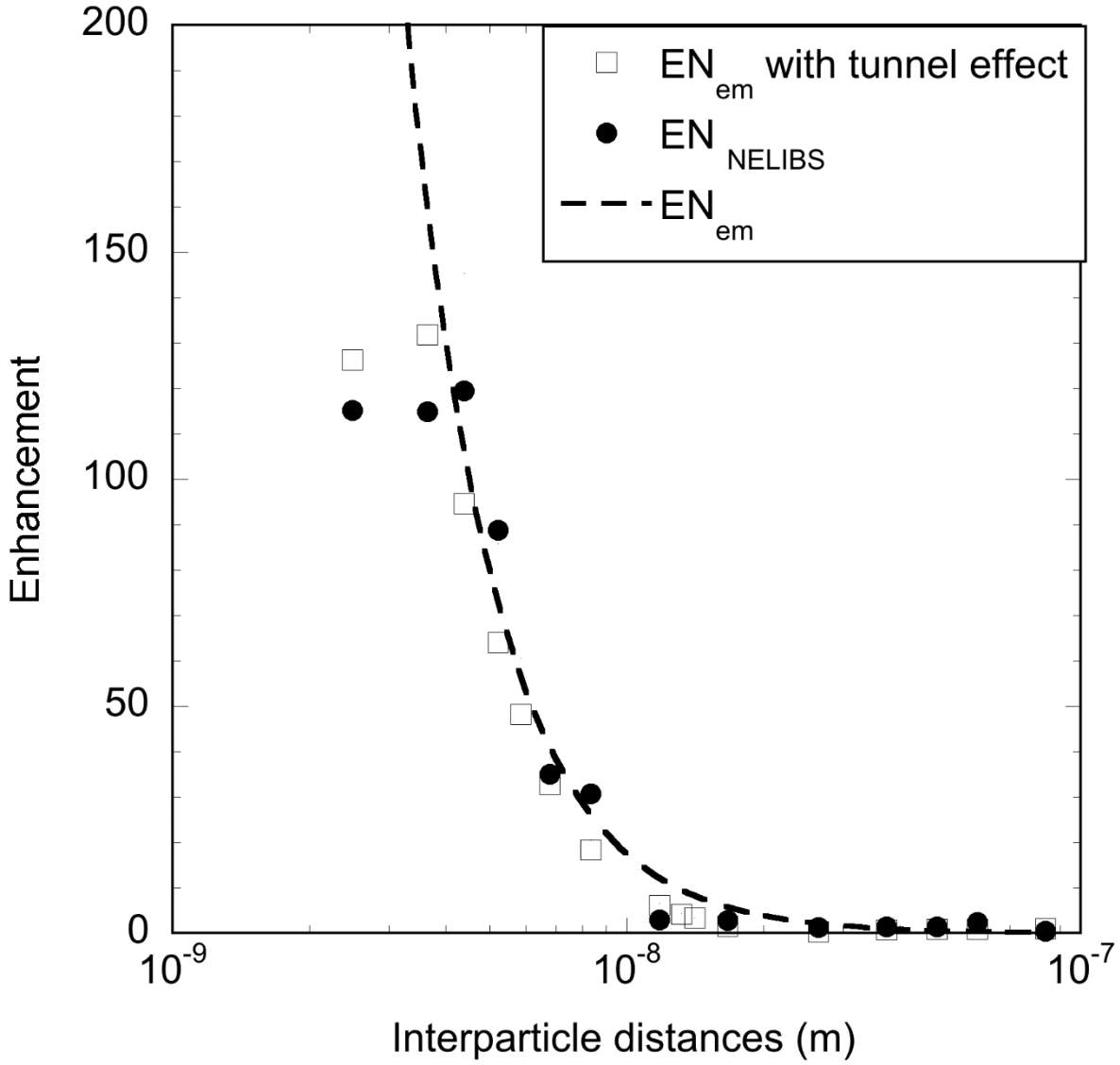

Fig.2. NELIBS signal enhancement (see Eq.1) of Ti I at 365.45 nm as a function of interparticle distance with 20 nm AgNPs deposited on a titanium sample, laser fluence: 13 J cm^{-2}, acquisition time: , delay: 200 ns, gate width: 1.2 µs. Experimentally observed NELIBS enhancement (full circles); theoretical field enhancement as calculated from Eq. 2 with (empty squares) and without (dashed lines) correction for tunnel effect.

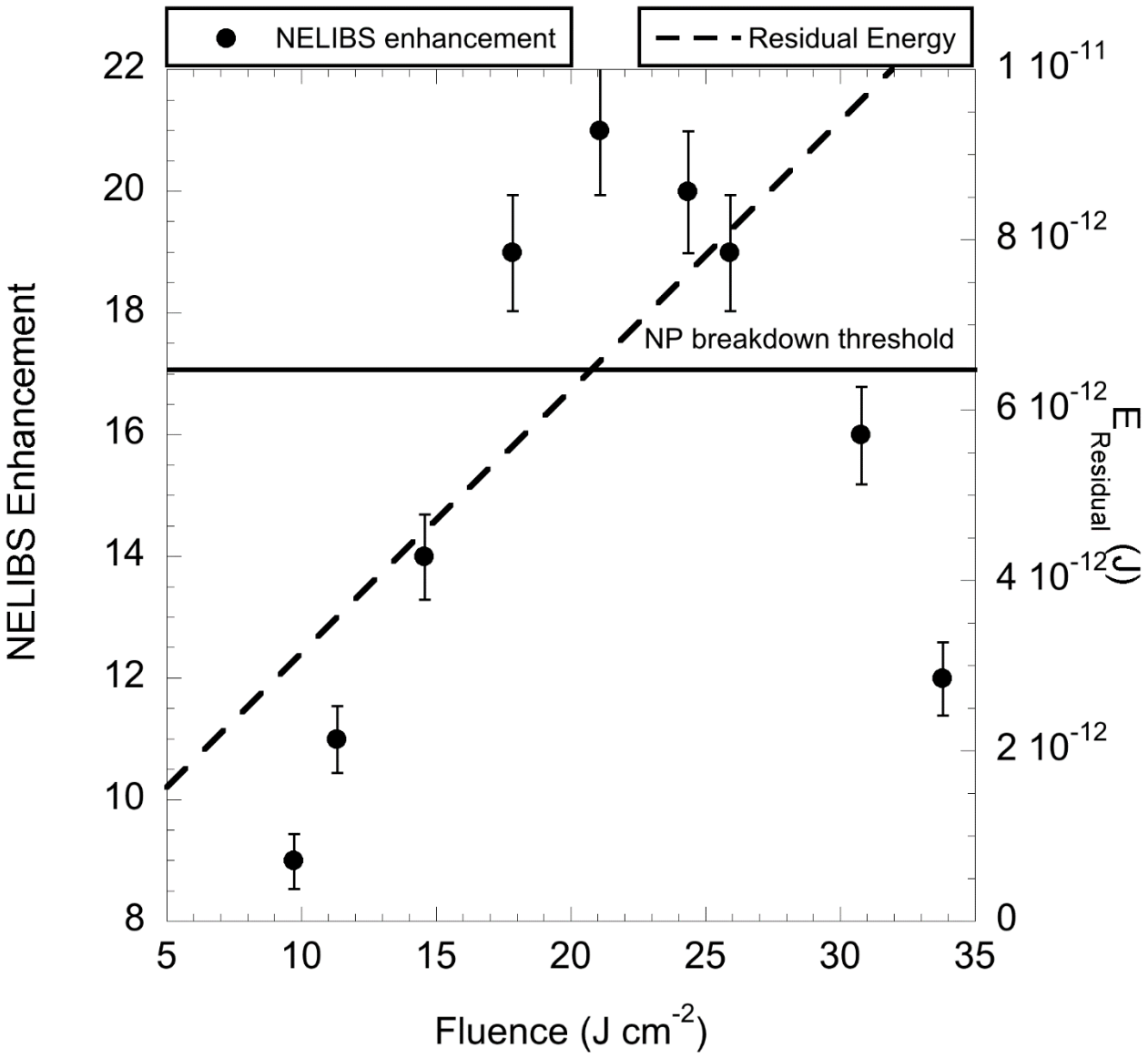

Fig.3. Dependence on fluence of a) calculated residual energy from Eq.7 (dashed line) as function of the laser fluence assuming α=1, N_{NP}= 3 10^9, EN=22.7, r_{hot}=1 nm, R=10 nm and b) experimental enhancement (Full circles) with standard deviation from Ref.[7] under the following experimental conditions: Ag NPs were deposited on a Ti sample (NP diameter: 20 nm and number of irradiated NPs: 3 10^9).

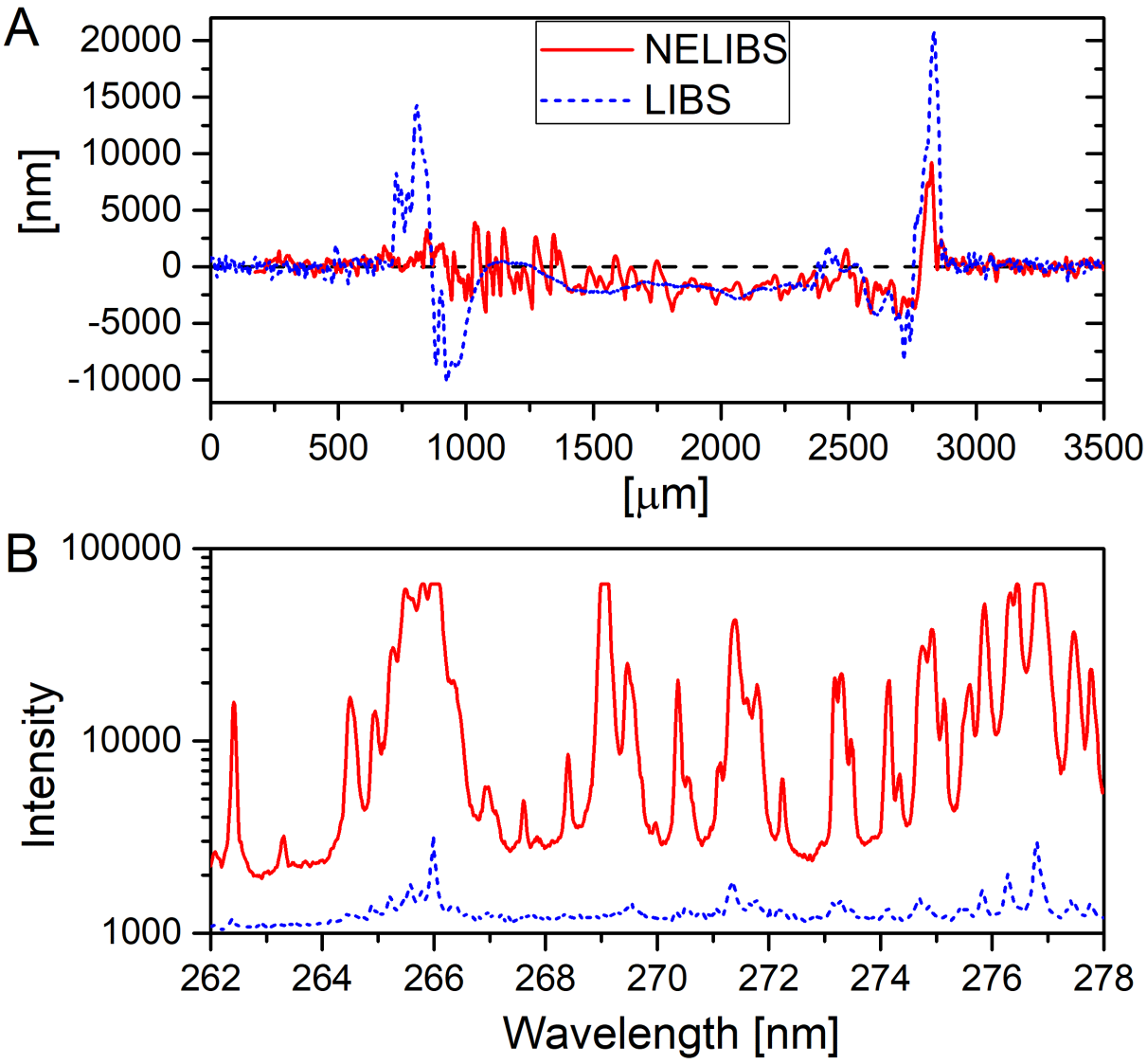

Fig.4. a) Crater analysis was performed with a stylus profilometer, Alpha-step D-120 (KLA-Tencor, Milpitas, CA) after 50 shots of NELIBS and LIBS on titanium. b) Corresponding emission spectra under the following experimental conditions: fluence: 5 J cm^{-2}, delay: 1 μs, gate width: 5 μs, 1μl of AuNPs (0.126 mgl^{-1}; 7 nm diameter) produced by PLAL with a surface concentration of 4.0 10^{-3} mg cm^{-2} on the target surface. In the case of NELIBS after each shot a new NPs deposition was done.

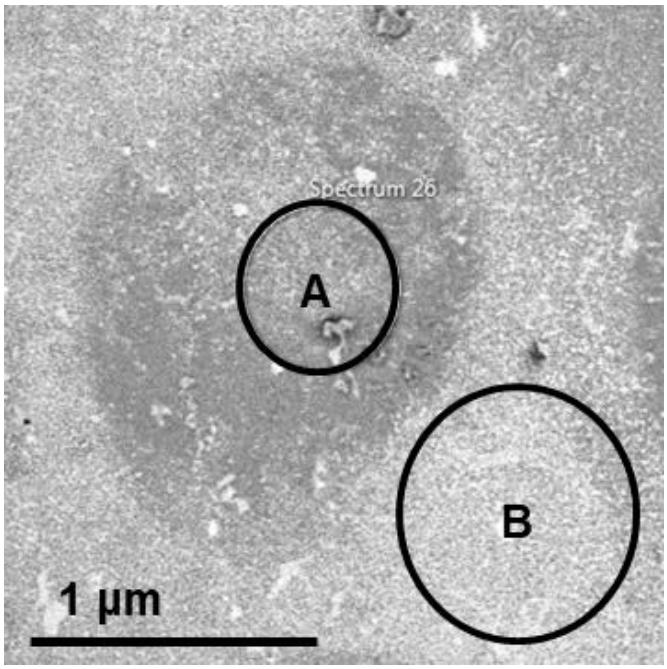

Fig.5. Scanning electron microscope (SEM) images of an aluminum based alloy surface covered with 10 nm Au-NPs. MIRA3 (Tescan, Czech Republic). The sample was measured using secondary emission mode (in-beam detector) at 15 kV, depth regime and working distance of 7 mm. Zone A is in a region inside the ablated area, while zone B is in an area outside the ablated area. Elemental analysis was provided by Energy-dispersive X-ray spectroscopy (EDX), working distance 15 mm, visualized with a BSE detector and a 50 mm SDD detector (Oxford Instruments, UK) was used. Data were evaluated using Aztec software ver. 3.1 (Oxford Instruments, UK) and the Au abundance in mass was 1.7 % and 7.9 % respectively for the zones A and B.

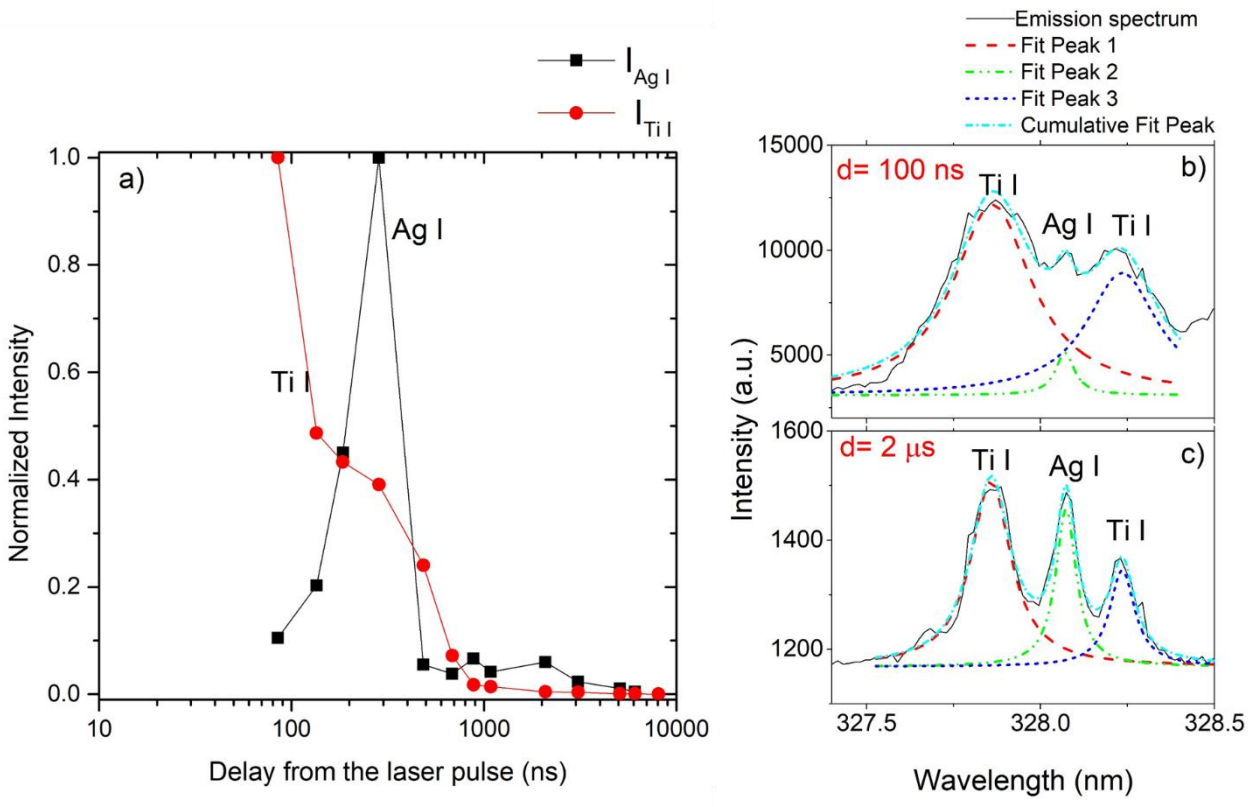

Fig.6. a) Temporal evolution of the atomic emission intensity of Ag I 328.07 nm and Ti I 327.7 nm, normalized to the maximum emission signal, during NELIBS on titanium with 20 nm AgNPs at a laser irradiance of 13 J cm^{-2}. b) and c) show sections of two emission spectra acquired at delay 100 ns and 2 μs, respectively, where the Ag I and Ti I emission lines are in evidence.

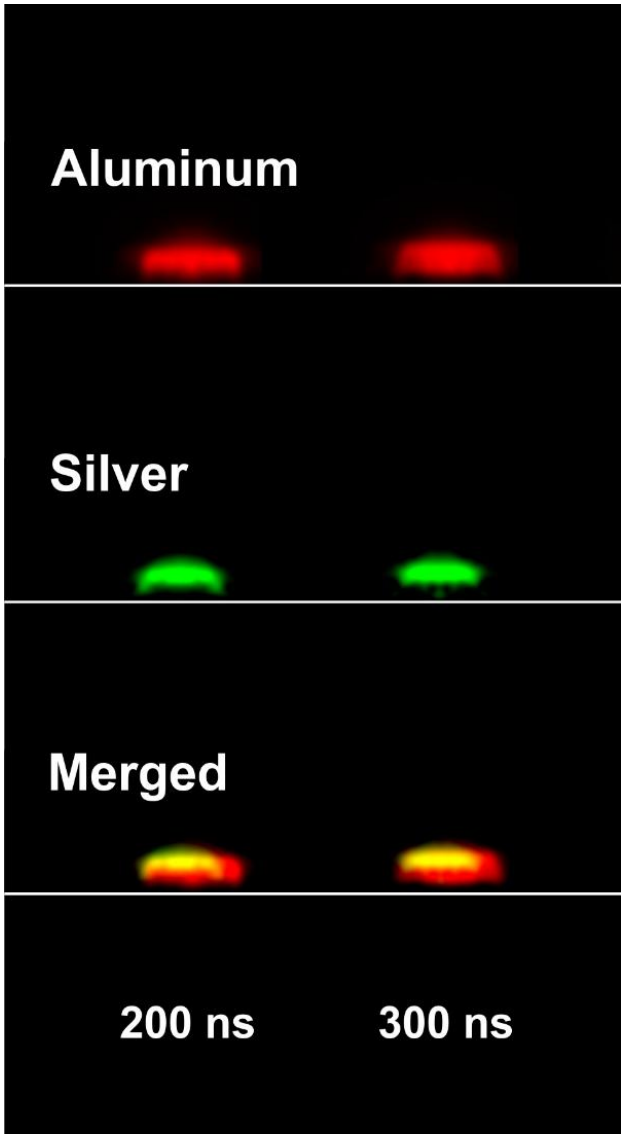

Fig.7. Spectrally resolved images of NELIBS with 20 nm AgNPs on an Al target. The green color represents the emission of Ag I 328.07 nm and the red color represents Al I 396.15.

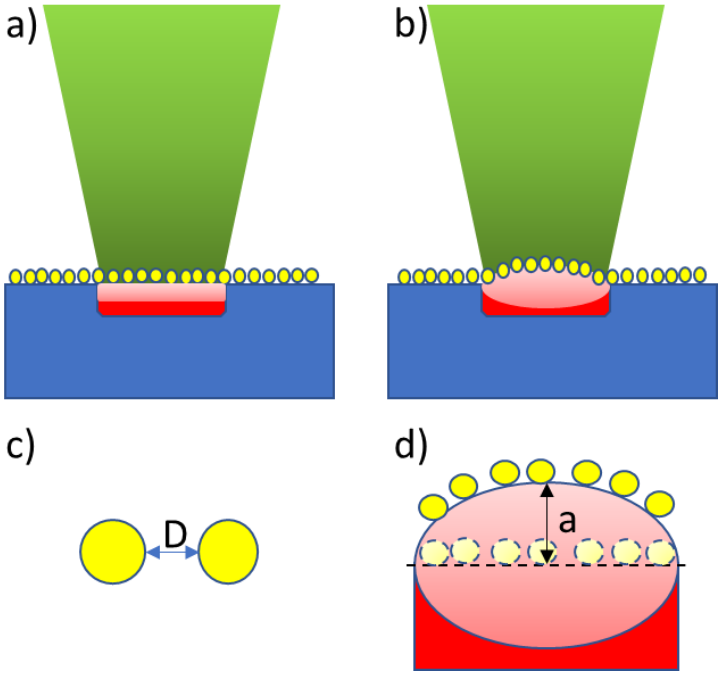

Fig.8. The material expansion of a target (blue) during the laser pulse (green) and its effect on the NP interparticle distance: a) The moment the laser reaches the target surface the interaction area is a flat circle (pink); b) During the laser irradiation the material expands to an oblate spheroid volume; c) The interparticle distance (D) between two adjacent NPs (yellow); d) The effect on the distance between the NPs with the expansion of the laser interaction surface from a flat circular (dashed line) to oblate spheroid (blue ovoid) shape with minor semi-axis a.

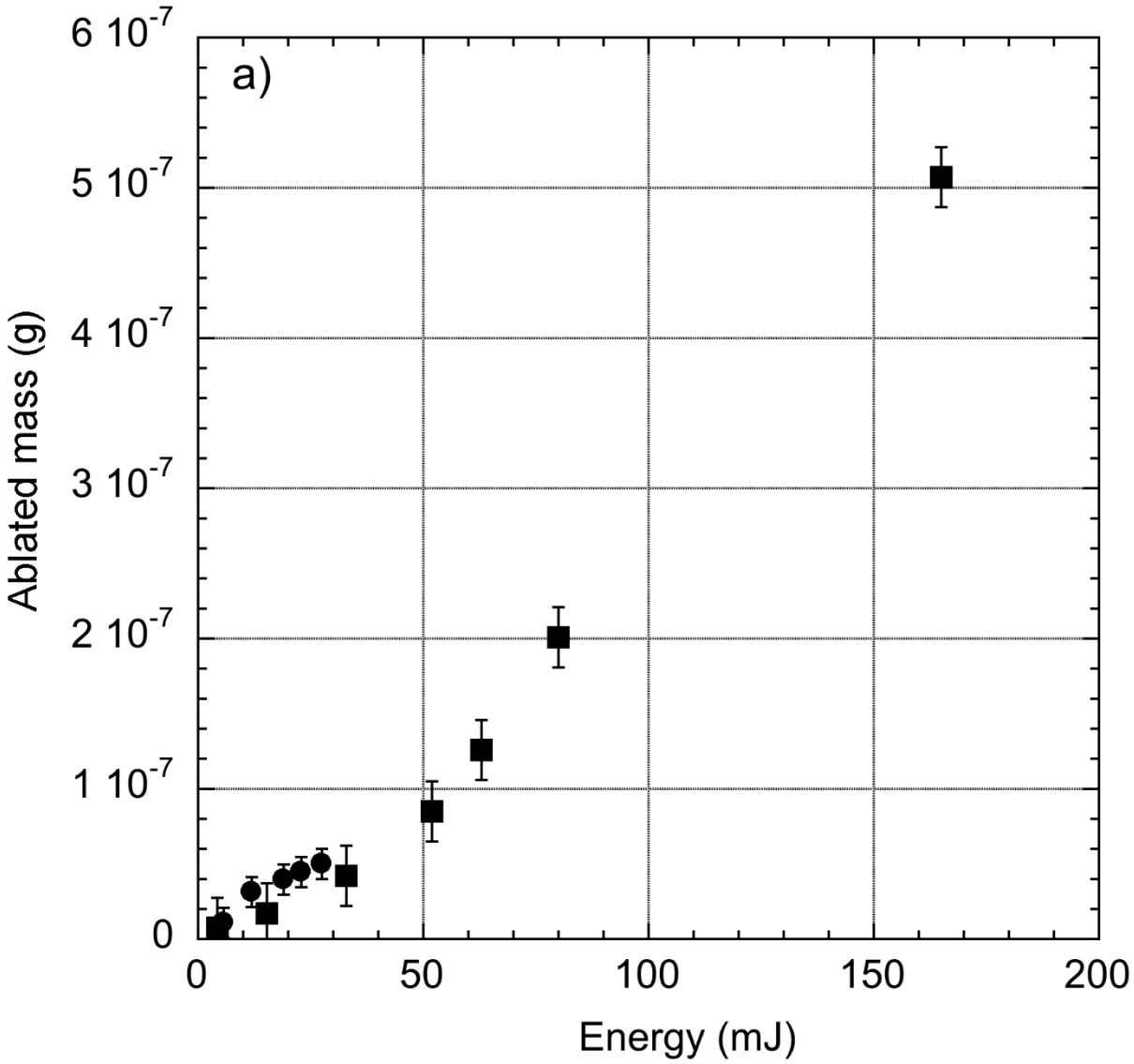
a)
Ablated mass (g)
6 10-7
5 10-7
4 10-7
3 10-7
2 10-7
1 10-7
0
0
50
100
150
200
Energy (mJ)

Fig.9a

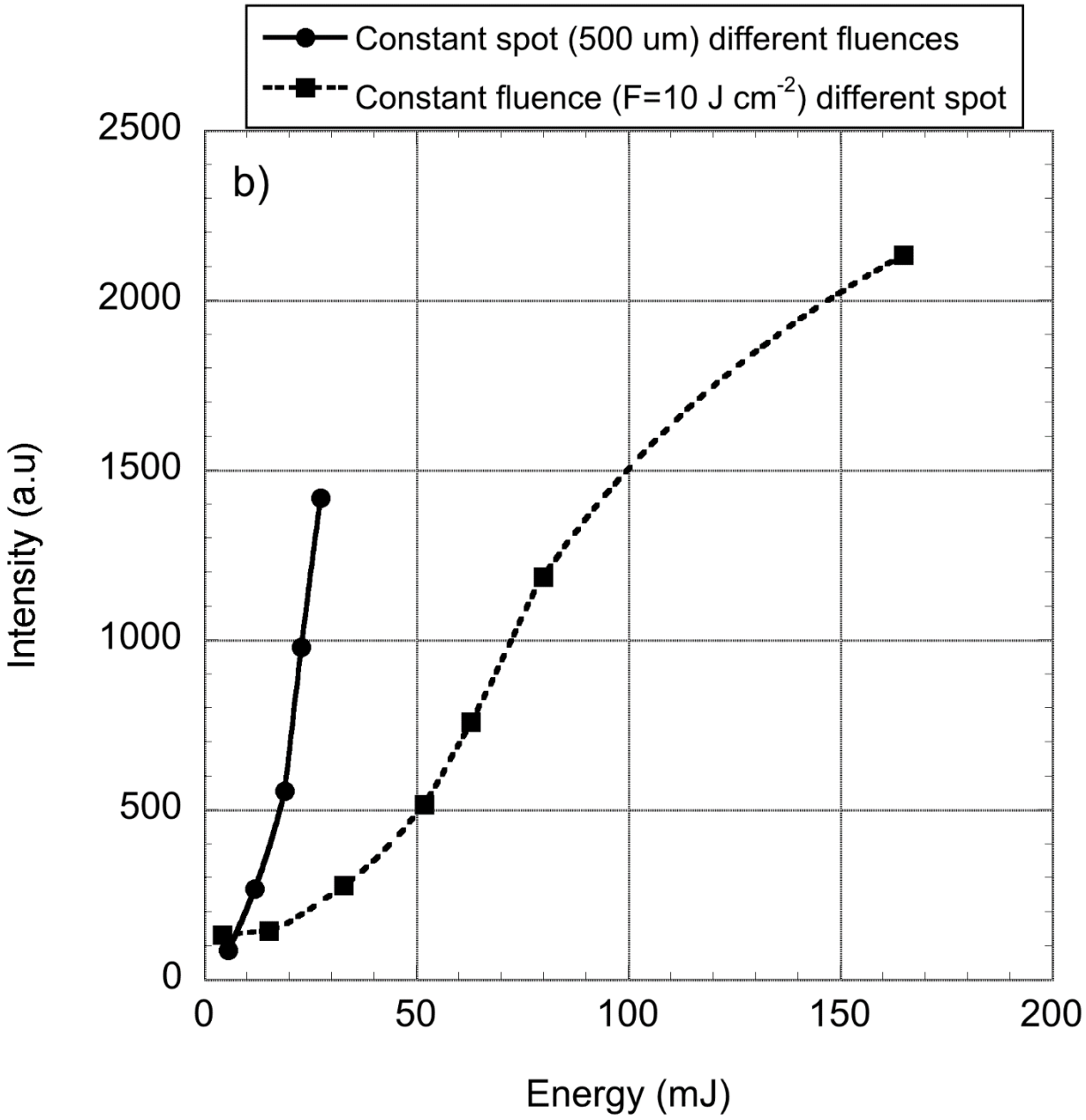
Constant spot (500 um) different fluences
Constant fluence (F=10 J cm-2) different spot
b)
Intensity (a.u)
Energy (mJ)
0
500
1000
1500
2000
2500
0
50
100
150
200

Fig.9b

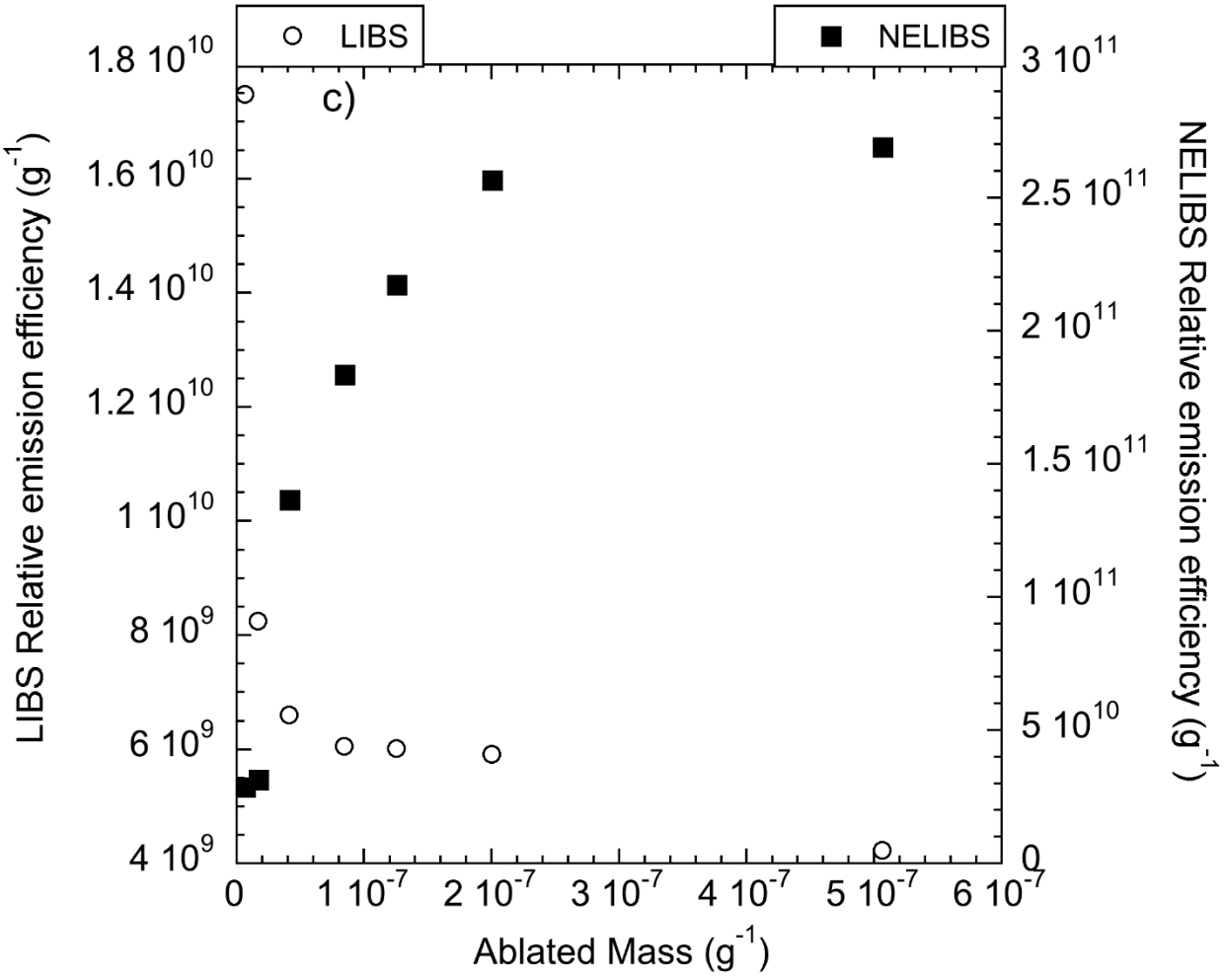
LIBS
NELIBS
c)
LIBS Relative emission efficiency (g^{-1})
NELIBS Relative emission efficiency (g^{-1})
Ablated Mass (g^{-1})
1.8 10^{10}
1.6 10^{10}
1.4 10^{10}
1.2 10^{10}
1 10^{10}
8 10^{9}
6 10^{9}
4 10^{9}
3 10^{11}
2.5 10^{11}
2 10^{11}
1.5 10^{11}
1 10^{11}
5 10^{10}
0
0
1 10^{-7}
2 10^{-7}
3 10^{-7}
4 10^{-7}
5 10^{-7}
6 10^{-7}

Fig.9c

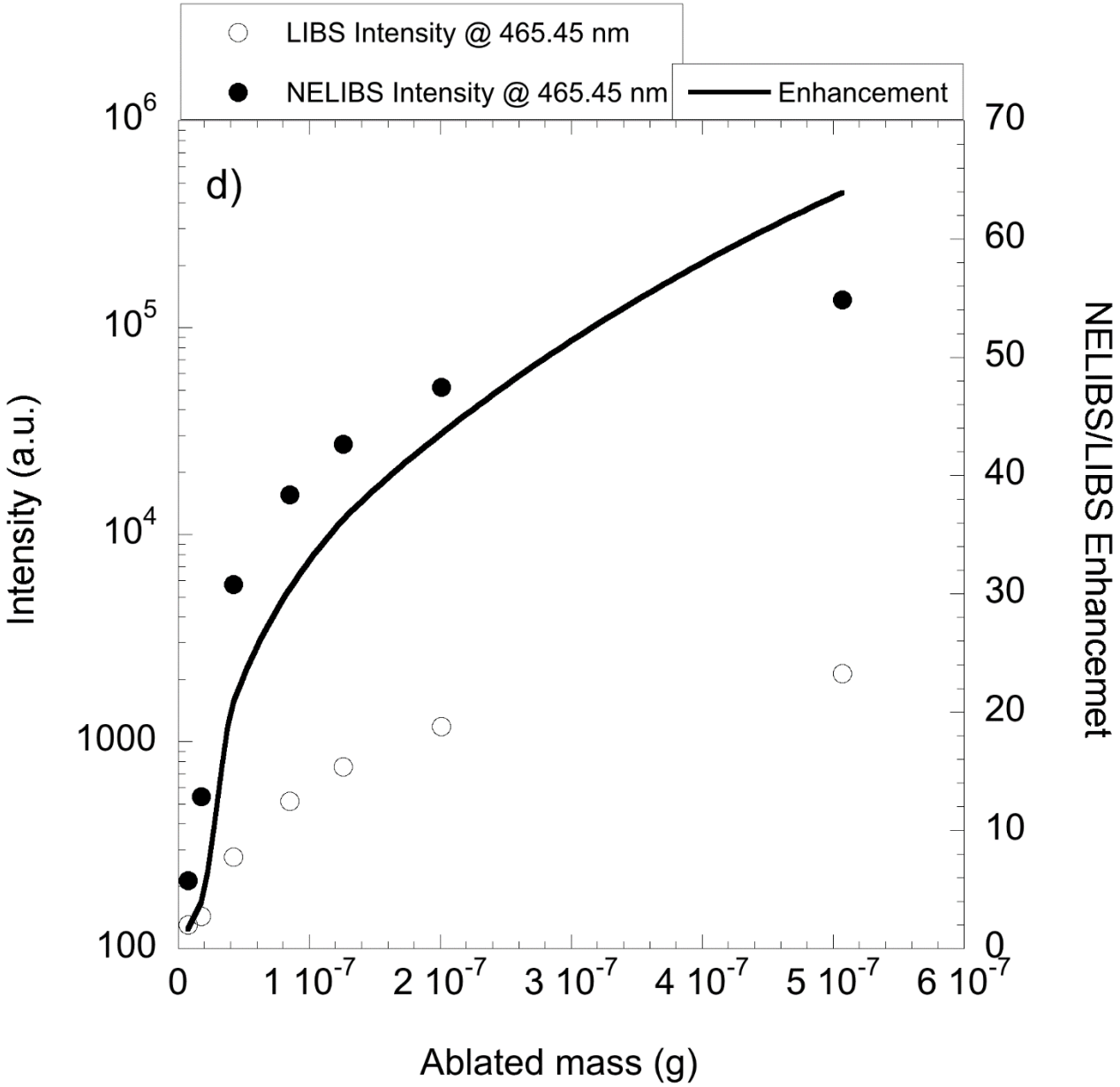

Fig.9d

Fig.9. Effect of laser fluence and spot size on intensity and ablated mass a) Dependence of the ablation mass and relative error as function of laser energy keeping constant the spot size and varying the laser fluence (circles) and keeping constant the laser fluence but varying the spot size (squares); b) Dependence of the intensity of Ti I 462.3 nm as function of laser energy keeping constant the spot size and varying the laser fluence and keeping constant the laser fluence but varying the spot size; c) Dependence of relative emission efficiency (Intensity/ablated mass) as function of the ablated mass in LIBS and NELIBS; d) Intensity and NELIBS enhancement as function of the ablation mass. For NELIBS 1µl of AuNPs (0.126 mgl^{-1}; 7 nm diameter) produced by PLAL with a surface concentration of 4.0 10^{-3} mg cm^{-2} on the target surface have been used.

Expansion velocity (m s^{-1})	Expansion distance after 6 ns (m)	NP interparticle distance (m)
Before the laser shot		$7.9\ 10^{-9}$
$1\ 10^{4}$	$6\ 10^{-5}$	$8.3\ 10^{-9}$
$5\ 10^{4}$	$3\ 10^{-4}$	$1.2\ 10^{-8}$
$1\ 10^{5}$	$6\ 10^{-4}$	$1.7\ 10^{-8}$
$1\ 10^{6}$	$1\ 10^{-3}$	$2.4\ 10^{-7}$

Tab.1. Calculated interparticle distance of 20 nm NPs as function of the plasma expansion velocity considering the expanded matter resembling an oblate spheroid during the 6 nm laser irradiation pulse as illustrated in Fig.8.